

of flow in? Temporal Evolution in the Networks of Porous Materials: From Homogenization to Instability

Ahmad Zareei, Deng Pan, and Ariel Amir*

School of Engineering and Applied Sciences, Harvard University, Cambridge, MA, 02148

(Dated: February 23, 2021)

We study the dynamics of flow-networks in porous media using a pore-network model. First, we consider a class of erosion dynamics assuming a constitutive law depending on flow rate, local velocities, or shear at the walls. We show that depending on the erosion law, the flow may become uniform and homogenized, stay as it is, or become unstable and develop channels. Using a simple model, we identify quantitative criteria to distinguish these regions. By defining an order parameter capturing different behaviors we show that a phase transition happens depending on the erosion law. Lastly, we show that pores clogging at the initial stages show different behaviors depending on clogging dynamics, however, due to the pore throat blockages and changes in the network connections the behavior diverges from predicted behavior.

regimes

misleading confusion?

regimes be linear?

Fluid flow through a porous medium undergoing a dynamical change in its network of micro-structure is a challenging problem and has many environmental and industrial applications, such as oil recovery [1, 2], CO₂ sequestration [3], water filtration/separation [4–8], energy storage [9, 10], or biological applications [11–14]. Fluid flow throughout a porous medium is often heterogeneously distributed between the pores as a result of a highly disordered pore structure. Due to the fluid flow, the pore structure can further change dynamically either through the erosion of pore boundary walls or deposition/sedimentation of material on the boundary of the pores. Such heterogeneous dynamical changes affect the pore-level fluid flow which in turn affects the dynamical changes to the pore structure. This feedback mechanism along with the initial heterogeneous fluid flow complicates the dynamical process and makes it difficult to understand and predict the porous media behavior. Nonetheless, an understanding of the dynamical change is essential to improve any of the porous media applications where the pore network changes over time, applications such as groundwater remediation and precipitation of minerals in rocks [15], biofilm growth in water filtration, and protective filters [4–8], as well as enhanced oil recovery with polymer flooding [16, 17], or water-driven erosion [18, 19].

In light of the plethora of applications, it is surprising that the evolution of porous structures exposed to erosion and deposition has only been partially understood both theoretically and experimentally. In order to model erosion in porous materials, various models have been used where erosion locally is proportional to different flow parameters. Some studies have focused on the erosion of the pore structure proportional to the shear stress at the walls [20], or proportional to the power dissipated [21]. More recently it has been shown that an erosion proportional to the local fluid flux [22] can effectively result in branching/channelization of the porous media. Similarly,

in clogging, deposition rate based on local fluid flux [23], velocity [24], or even at a constant rate independent of flow parameters [25] has been used. Despite all of the different models, a consensus on the dynamics of erosion or clogging is missing.

Here we use a phenomenological discrete network-based model [26–29] to model the hydrodynamically driven erosion or clogging in a porous material. The network of pores inside the solid structure is connected together through pore throats that effectively show resistance to the fluid flow between the pores (Fig. 1a). In a network model, the pores/voids of the porous medium are represented by a two- or three-dimensional lattice of nodes. The edges between the nodes of the network represent the pore-throat between the pores and are modeled using cylindrical tubes characterized by their radius and length. Network-based models have successfully shown to capture key properties of fluid flow in a porous material such as the probability distribution of fluid flux [26], the permeability scaling during clogging [30], or the first fluidized path in a porous structure [31]. In order to study erosion in such network models, the degradation of the solid skeleton or clogging of pores is taken into account by the change (increase or decrease) in the resistance of the edges between the pores. Using a general local erosion law that can model different dynamics, we show a variety of behaviors are possible. The network can either move toward stability and homogenization, stay as it is with no significant change in network statistics, or even become unstable and develop channels. Using numerical solutions with erosion model on a random network we show the emergence of two behaviors and morphologies are possible through selective erosion and subsequent flow enhancement. Using a simplified model we capture the underlying physics and furthermore show a phase transition occurs depending on the parameters of the model.

Methods and Results—We consider low-Reynolds fluid flow through the porous network, i.e., $\rho u l / \mu \ll 1$ where ρ is the fluid density and μ is the kinematic viscosity, u and l are characteristic fluid velocity and pore length. In such conditions, the fluid flow in each tube follows Poiseuille law $p_i - p_j = (8\mu l_{ij} / \pi r_{ij}^4) q_{ij}$ where p_i, p_j repre-

* arielamir@seas.harvard.edu

[here and elsewhere
add a space?
(check PCL format?)]

shape
be
radius
I
think.

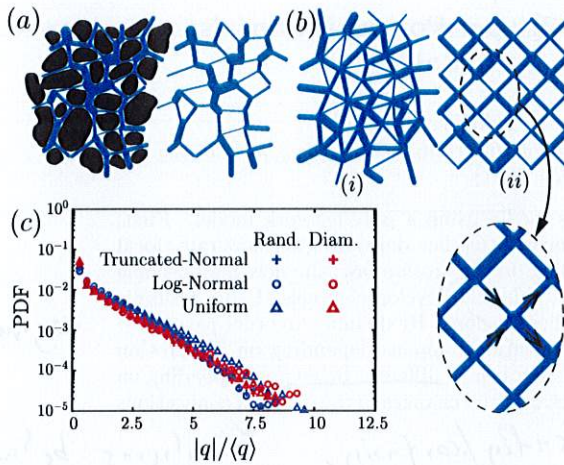


FIG. 1. (a) Cross section of a porous media obtained using computerized tomography (CT) scan of a sandstone sample (CT image taken from [32]). The network of pores and throats is highlighted in blue. In the network model, the pores are represented with nodes and the throats between pores are approximated with tubes connecting the pores together. (b) Schematic of a topologically random network (i); and a structured diamond grid network (ii). The edge diameters in both networks are randomly distributed. The inset figure shows the conservation of mass at each node. (c) The universal probability distribution function (PDF) of fluid flux for a topologically random (in blue) or diamond network (red) with a highly disordered random net including uniform (triangles), log-normal (circles), and truncated normal (plus) distributions. In all distributions, the coefficient of variation is set to 0.5. Generally, in a highly disordered random network, the PDF of normalized fluid flux becomes independent of the network and follows a universal distribution with an exponential tail.

sents pressures at neighboring nodes i , j , and r_{ij} , l_{ij} , q_{ij} are respectively the radius, length, and fluid flow rate at the edge connecting pores i and j . The coefficient $\pi r_{ij}^4 / 8\mu l_{ij}$ which relates the fluid flux to the pressure difference can be considered as the conductance C_{ij} of the edge ij in the pore-network. In addition to Poiseuille flow at the edges, the total incoming flow at a node should be equal to the total outgoing flow ~~or the mass should be conserved~~. The conservation of mass at pore i can be written as $\sum_{j \in N(i)} q_{ij} = 0$ where $N(i)$ represents all the neighboring nodes of node i . First, we consider a topologically random network of nodes constructed using a uniform distribution of $N_x \times N_y$ nodes in a planar domain $[0, L_x] \times [0, L_y]$ where the nodes connectivity are obtained using Delaunay triangulation (see Fig. 1b for a part of such network). The radius of the edges are considered as independent and identically distributed random variables sampled from a probability distribution that can be either uniform, log-normal, or a truncated normal distribution (see supplementary material for more details). Assuming a pressure difference between the boundary nodes at the left and the right

boundary, the pressure at the nodes, and the fluid flow rate at the tubes can be obtained by solving the corresponding set of linear equations. We find that for large enough randomness in the edge radius between the pores (i.e., $\text{std}(r_{ij})/\text{mean}(r_{ij}) \geq 0.5$), the PDF is well described by a single exponential distribution as shown in Fig. 1c. The exponential form of the PDF reflects the relatively small number of extremely large fluid flux. The exponential distribution of fluid flux obtained here is similar to the earlier experimental or numerical measurements [26, 30, 33]. Next we consider a structured diamond-grid of pores (Fig. 1b) which significantly simplifies the geometrical complexity of the network. We find that the PDF of normalized fluid flux remains unchanged in such networks for various distributions (Fig. 1c). The diamond grid allows us to analytically track the propagation of fluid into the network and calculate the distribution of fluid flux using a mean-field approximation (see supplementary material). Using a similar idea proposed for the force distribution in granular materials [34, 35], we find that the PDF of normalized fluid flux inside a highly disordered porous material converges to a universal distribution with an exponential form, i.e., $p(\hat{q}) \propto e^{-\alpha\hat{q}}$ for large \hat{q} where \hat{q} is the normalized fluid flux $\hat{q} = q/\langle q \rangle$ (see supplementary materials). As a result, the diamond grid network of pores where cylindrical edges between the pores have a highly disordered distribution of diameters is enough to capture the statistics of a heterogeneous fluid flow inside a porous material.

In order to model the erosion in porous media, we consider the abrasion in the throats which correspond to the change in the radius of the edges in the network. We model the dynamics of the change in the radius as

$$\frac{dr_{ij}}{dt} = \alpha \frac{q_{ij}}{r_{ij}^n} \quad (1)$$

where n is an integer number and c is a constant. Different powers of n correspond to different physics in the erosion. Particularly, when (i) $n = 0$ the erosion depends on the amount of flux q_{ij} passing through the edge; (ii) $n = 2$ the erosion depends on the local velocities; (iii) $n = 3$ the erosion depends on the shear force at the boundary of the throat. We consider the diamond-grid network initialized with a size of $N_x \times N_y$ tubes in the horizontal and vertical directions. We initialize the network with a uniform random distribution of diameters within $[r_{\min}, r_{\max}]$ range with a large coefficient of variation such that $\sigma_r/r_0 \approx 0.5$ where σ_r is the standard deviation, and $r_0 = \langle r \rangle$ is the mean radius of the tubes. This large coefficient of variation corresponds to the highly disordered porous media. The flow inside the pores, PDF of flux in the tubes, and PDF of tube radii are shown in Fig. 2. We assume a constant pressure difference between the left and the right boundaries. In each time step, we increase the local radius of the tubes based on the erosion law introduced in Eq. (1). Note that $r_{ij}(t+1) = r_{ij}(t) + (\alpha\delta t)q_{ij}(t)/r_{ij}^n(t)$, where the coefficient $\alpha\delta t$ is chosen such that the maximum change in

where?

how
to?
what
about
Karen
Alain
work?

the radius at each time step is smaller than one-tenth of the smallest tube's radius i.e. $\max(\Delta r_{ij}) \leq r_{\min}/10$ of the smallest radius at the initial configuration. This condition guarantees that at each step a small amount of material is eroded and there's no sudden change in the network. We further test that the result is converged and decreasing $\max(\Delta r_{ij})$ does not affect our result. To better capture the fate of the network we continue the simulations to the extreme values until when $\langle r \rangle = 2r_0$.

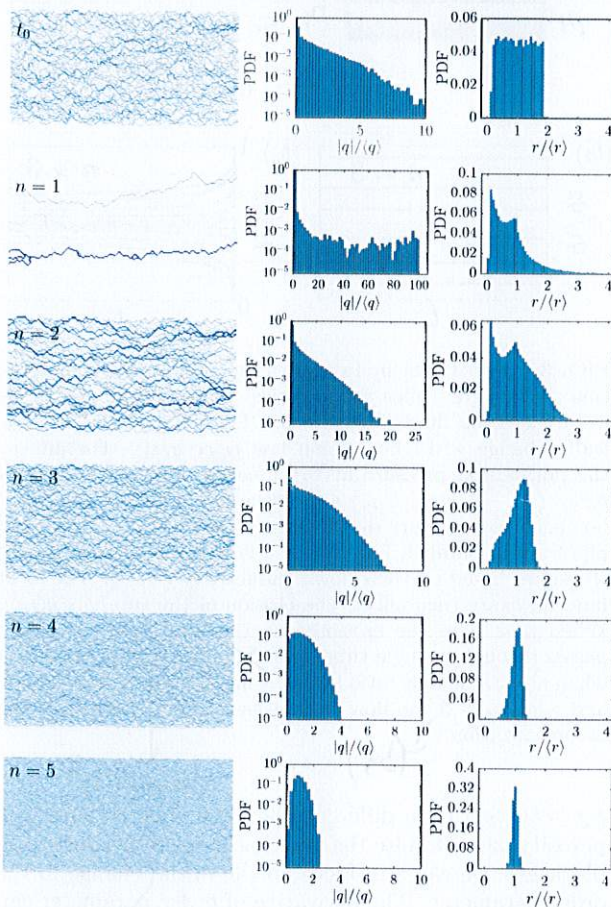


FIG. 2. Erosion in a network of pipes. The initial condition is shown with the label $t = 0$ in the first row. Each row afterward corresponds to the simulation result after N steps such that $\langle r_{t=N} \rangle = 2r_0$ where $r_0 = \langle r_{t=0} \rangle$ or twice the initial average radius, as a result in all cases the same amount of material is eroded. The erosion law is based on Eq. (1) where different powers of n correspond to different physics of erosion. The first column is a snapshot of the pore network, the second column is the PDF of normalized fluid flux $|q|/\langle q \rangle$, and the last column is the PDF of normalized radius $r/\langle r \rangle$.

The results of the simulations for different n are shown in Fig. 2. When $n = 1$ or 2, the erosion develops channels in the porous media, and channeling instability occurs. In such cases, the flow is dominated by a few edges carrying most of the flow while the rest of the network carries almost no flow. This can also be seen in the PDF of the

the network develops channels

not so evident,
I would rephrase.

normalized fluid flux which becomes bimodal: a few edges with very high flux values and the majority of the edges with very small flux. The distribution of diameters, similar to the PDF of fluxes, diverges into two parts, one with a few large diameters that form the channels and carry almost all the flow, while the rest and most of the tubes have very small radii. Contrary to $n = 1, 2$, when $n = 3$ and the erosion depends on shear at the throats' boundary walls, we find that the flow patterns stay very close to the initial shape, however, with larger and exacerbated flux values. Although the maximum fluid flux increases, the PDF of normalized fluid fluxes remains almost exponential, and the PDF of diameters moves toward larger values. Increasing n to larger values, $n = 4$ or 5, we find that the flow pattern in the network moves toward homogenization. Here, the tail of the normalized fluid flux distribution retracts and the distribution moves toward the average value. We further find that the PDF of the diameters moves toward the average and the coefficient of variation reduces. Running the simulations for longer times, we observe that the flow becomes completely uniform where only a single radius appears to carry the flow with the same fluid flux (i.e., the average value) for all the tubes in the network. In summary, we have observed a transition in the network behavior during erosion which happens at $n = 3$: when $n < 3$ the network moves toward developing channels, and when $n > 3$ the erosion results in the homogenization of the flow.

Simplified Model—In order to understand the underlying reason behind the transition in network behavior during erosion for different powers of n , we focus on a simplified model with only two tubes in parallel or series (see Fig. 3a,b). First, assuming two cylindrical tubes with radii r_1, r_2 in series and connected back to back, the flow is the same for the two tubes $q_1 = q_2 = q$ (Fig. 3a). The radius of each tube then changes with $dr_i/dt = \alpha q/r_i^n$ where $i = 1, 2$. Each tube can be considered as a resistor where its conductivity $C_i = \pi r_i^4/8\mu l_i$ changes over time. In similarity with resistor networks, pressure difference ΔP acts analogous to the voltage difference and the fluid flux q becomes analogous to the current where we have $q = C_i \Delta P$. When the cylindrical tubes are in series, we find that the conductivity of each tube changes as $dC_i/dt \propto q C^{(n-3)/4}$. As a result, each tube's conductivity increases with the rate depending on n , i.e. the larger the n the faster it moves toward larger values. If we consider the pressure at the junction between tubes, we find that this middle point pressure moves toward the average value of pressure on both sides. This suggests that when the tubes are in series, the erosion results in achieving a homogenized distribution of pressure. Contrary to tubes in series, when the tubes are in parallel (Fig. 3b), the flow divides between the two tubes based on their conductivity i.e. $q_1/q_2 = C_1/C_2$. Since each tube's radius changes as $dr_i/dt = \alpha q_i/r_i^n$, the evolution

$\Delta P_i, n?$

See ST
or
give
etc.
here?

dr_i/dt ?

From: 'The elements of style'
omit needless words

of the fluid flow ratio becomes

$$\frac{d}{dt} \left(\frac{C_1}{C_2} \right) \propto \frac{C_1}{C_2^{(n+1)/4}} \left(\left(\frac{C_1}{C_2} \right)^{\frac{n-3}{4}} - 1 \right). \quad (2)$$

When $n = 3$ in Eq. (2), the right-hand-side becomes zero and as a result the flow ratio C_1/C_2 remains constant and does not change. However, when $n \neq 3$, we find that $C_1/C_2 = 1$ is an equilibrium point. When $n > 3$ this equilibrium solution becomes unstable and the solution moves toward $C_1/C_2 \rightarrow 0/\infty$ which means that the whole flow passes through one of the tubes. To summarize, when the tubes are in series any erosion law makes flow become more uniform; however, when the tubes are in parallel depending on the power n the flow in the tubes can move toward becoming more uniform ($n > 3$), stay the same ($n = 3$), or move toward instability and channel development ($n < 3$). [This observation is consistent with the numerical simulation results shown in Fig. 2.]

Phase transition—In order to quantify the transition of the network between channeling instability and homogenization, we define an order parameter \mathcal{O} that moves toward 0 or 1 if the network moves toward channeling or homogenization respectively. The order parameter is defined as

$$\mathcal{O} = \frac{1}{N-1} \left(N - \frac{\left(\sum_{ij} q_{ij}^2 \right)^2}{\sum_{ij} q_{ij}^4} \right) \quad (3)$$

where N is the number of edges. The order parameter $\mathcal{O} = 0$ when the flux in all the edges become the same $q_{ij} = \bar{q}$. On the other hand, when fluid flux becomes highly localized with only a few edges with non-zero flux, $\mathcal{O} \rightarrow 1$. We numerically calculated the order parameter \mathcal{O} for the diamond-grid network during the erosion process. The results are shown in Fig. 4 for different amounts of erosion measured by the increase in the average diameter $\langle r \rangle / r_0$. As shown in Fig. 4, at $n = 3$ the order parameter remains unchanged; however for $n > 3$ the order parameter moves toward zero, where the flow becomes more uniform and for $n < 3$ the order parameter goes toward unity, where channels are developed. The transition in the order parameter indicates a phase transition at $n = 3$ in the long time behavior of the network which is in agreement with the toy model prediction and simulation results in Fig. 2.

Clogging Dynamics—Besides erosion, another change in the network is the deposition/sedimentation of material on the boundary walls of the porous material. We name this dynamical change a “clogging” process as opposed to erosion. Contrary to erosion, the clogging behavior causes the edges to block which effectively alters the network of connectivity and network behavior. This change in the connection between nodes through edges getting blocked can drastically alter porous structure behavior,

what is being
Figure can
be improved.
converging?

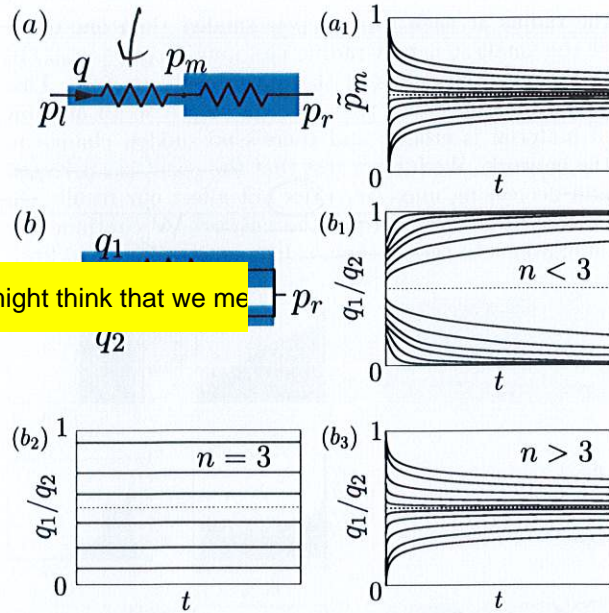


FIG. 3. Two tubes in (a) series or (b) parallel configuration. When the tubes are in series configuration, the tubes have the same fluid flow rate q . The tube radius dynamically changes with the erosion law $r_i \propto q/r_i^n$. For any n , the normalized pressure at the junction between the tubes $\tilde{p}_m = (p_m - p_l)/(p_r - p_l)$ approaches $1/2$ which results in a homogenized pressure distribution shown in (a₂). When the pipes are in parallel, however, the flow is distributed among the tubes based on their flow conductivity C_1, C_2 . The local fluid flow rate then affects the erosion of the tube $i \propto q_i/r_i^n$. When $n < 3$ in the erosion law, the fluid flow eventually passes through a single tube, and branching occurs. (b₂) when $n = 3$, the flow ratio between the pipes does not change, and when $n > 3$ the flow ratio approaches $1/2$ which is the homogenization.

channeling?

e.g., causes a huge difference between effective and true porosity [30]. Despite the drastic change of network with blockages, we can still focus on the initial change in the order parameter. The derivative of order parameter can be written as

$$\frac{d\mathcal{O}}{dt} = \sum_{ij} \sum_{kl} \frac{\partial \mathcal{O}}{\partial q_{ij}} \frac{\partial q_{ij}}{\partial C_{kl}} \frac{\partial C_{kl}}{\partial t} \quad (4)$$

where the last term changes from erosion to clogging, i.e., $\partial C_{kl}/\partial t = \pm \alpha \pi q_{kl}/r_{kl}^{n-3} \mu_{kl}$ for erosion and clogging respectively. As a result, the change in the order parameter is the negative of the erosion. Note that in Eq. (4), the second term depends on the network topology and pore throat clogging results in the change of network topology at large times. In short times, however, similar to the erosion, a phase transition exists at $n = 3$. When $n < 3$ the network moves toward homogenization during the clogging process and when $n > 3$ the flow moves toward the development of channeling instability. This initial direction, however, might not hold true at later times.

magnitude

equals
part of

* Somewhat abrupt transition:

Can you speculate on why it works?

e.g. Since complex networks include both series & parallel elements we expect...

fix
may
cause?
Some

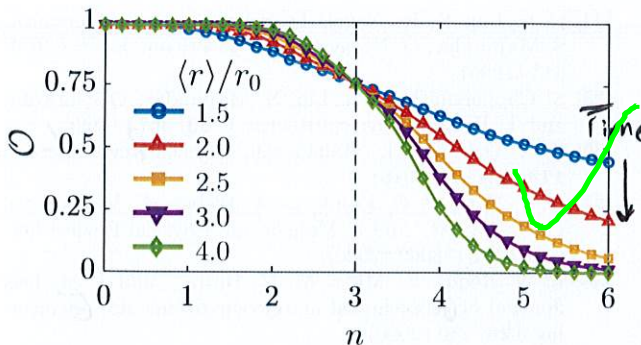


FIG. 4. Order parameter \mathcal{O} for different powers of n plotted over time as the network structure is eroded and average edge radius is increasing $\langle r \rangle / r_0$. When $n < 3$ the order parameter increases ($\mathcal{O} \rightarrow 1$) while the network is developing channels, and when $n > 3$ the order parameter decreases ($\mathcal{O} \rightarrow 0$) while the network moves toward homogenization, and when $n = 3$ the order parameter stays as it while the network statistics remains unchanged.

due to the complex changes in the connectivity network during the clogging process.

Conclusion—In summary, we analyzed the dynamics of the porous networks during erosion. We showed that depending on different erosion laws various network behaviors are observable. We used simple erosion law, inspired by the proposed models so far, and showed that depending on the rate of erosion the network can either move toward homogenization or toward developing channeling instability. Next, we propose an order parameter to capture the phase transition behavior, and using a simplified model of two tubes we described the physical origin of the phase transition behavior. In the case of clogging, since the network connectivity can vary significantly our approach does not hold at large times, however, the initial variation can be captured using our model where the results similarly show a behavior change at $n = 3$. Interestingly, a phase transition in active porous structures between full blockage and channelling instability [36]. These results signifies the importance of local dynamics in long time global behavior which requires further investigation.

?? Not
seen before.

← + Discussons?

Acknowledgments—We would like to acknowledge MRSEC DMR-2011754 for the support.

Karli Institute.

- [1] D. Fragedakis, C. Kouris, Y. Dimakopoulos, and J. Tsamopoulos, Physics of Fluids **27**, 082102 (2015).
- [2] M. Sahimi, *Flow and transport in porous media and fractured rock: from classical methods to modern approaches* (John Wiley & Sons, 2011).
- [3] W. H. Schlesinger, Science **284**, 2095 (1999), <https://science.science.org/content/284/5423/2095>.
- [4] J. Herzig, D. Leclerc, and P. L. Goff, Industrial & Engineering Chemistry **62**, 8 (1970).
- [5] C. Tien and A. C. Payatakes, AIChE journal **25**, 737 (1979).
- [6] D. P. Jaisi, N. B. Saleh, R. E. Blake, and M. Elimelech, Environmental science & technology **42**, 8317 (2008).
- [7] M. Carrel, V. L. Morales, M. A. Beltran, N. Derlon, R. Kaufmann, E. Morgenroth, and M. Holzner, Water research **134**, 280 (2018).
- [8] J. D. Seymour, J. P. Gage, S. L. Codd, and R. Gerlach, Physical Review Letters **93**, 198103 (2004).
- [9] M. Duduta, B. Ho, V. C. Wood, P. Limthongkul, V. E. Brunini, W. C. Carter, and Y.-M. Chiang, Advanced Energy Materials **1**, 511 (2011).
- [10] H. Sun, J. Zhu, D. Baumann, L. Peng, Y. Xu, I. Shakir, Y. Huang, and X. Duan, Nature Reviews Materials **4**, 45 (2019).
- [11] S. Marbach, K. Alim, N. Andrew, A. Pringle, and M. P. Brenner, Physical Review Letters **117**, 178103 (2016).
- [12] A. Tero, S. Takagi, T. Saigusa, K. Ito, D. P. Bebbert, M. D. Fricker, K. Yumiki, R. Kobayashi, and T. Nakagaki, Science **327**, 439 (2010).
- [13] K. Alim, G. Amselem, F. Peaudecerf, M. P. Brenner, and A. Pringle, Proceedings of the National Academy of Sciences **110**, 13306 (2013).
- [14] L. L. Heaton, E. López, P. K. Maini, M. D. Fricker, and N. S. Jones, Proceedings of the Royal Society B: Biological Sciences **277**, 3265 (2010).
- [15] M. N. Rad, N. Shokri, and M. Sahimi, Physical Review E **88**, 032404 (2013).
- [16] L. W. Lake, R. Johns, B. Rossen, G. A. Pope, et al., (2014).
- [17] S. Parsa, E. Santanach-Carreras, L. Xiao, and D. A. Weitz, Physical Review Fluids **5**, 022001 (2020).
- [18] N. Schorghofer, B. Jensen, A. Kudrolli, and D. H. Rothman, Journal of Fluid Mechanics **503**, 357 (2004).
- [19] A. Mahadevan, A. Orpe, A. Kudrolli, and L. Mahadevan, EPL (Europhysics Letters) **98**, 58003 (2012).
- [20] W. Hacking, E. VanBavel, and J. Spaan, American Journal of Physiology-Heart and Circulatory Physiology **270**, H364 (1996).
- [21] H. Steeb, S. Diebels, and I. Vardoulakis, “Modeling internal erosion in porous media,” in *Computer Applications In Geotechnical Engineering*, pp. 1–10, [https://ascelibrary.org/doi/pdf/10.1061/\(ASCE\)1943-5622.0002916](https://ascelibrary.org/doi/pdf/10.1061/(ASCE)1943-5622.0002916).
- [22] Assuming a mean-field approximation, local fluid flux becomes proportional to the pressure gradient. A local erosion rate using a threshold on the mean-field values of the pressure gradient is used in [19, 37].
- [23] H. Yang and M. T. Balhoff, AIChE Journal **63**, 3118 (2017).
- [24] The clogging rate in [38] assuming a dilute solution and initial times becomes proportional to local fluid velocity.
- [25] G. Boccardo, D. L. Marchisio, and R. Sethi, Journal of Colloid and Interface Science **417**, 227 (2014).
- [26] K. Alim, S. Parsa, D. A. Weitz, and M. P. Brenner, Physical Review Letters **119**, 144501 (2017).
- [27] I. Fatt et al., Transactions of the AIME **207**, 144 (1956).
- [28] M. J. Blunt, B. Bijeljic, H. Dong, O. Gharbi, S. Iglauber,

missed
ref.

fix.

not
sure
if
this
level
of
detail
is
right
here?

if
this
level
of
detail
is
right
here?

- P. Mostaghimi, A. Paluszny, and C. Pentland, *Advances in Water resources* **51**, 197 (2013).
- [29] N. Stoop, N. Waisbord, V. Kantsler, V. Heinonen, J. S. Guasto, and J. Dunkel, *Journal of Non-Newtonian Fluid Mechanics* **268**, 66 (2019).
- [30] S. Parsa, A. Zareei, E. Santanach-Carreras, E. Morris, A. Amir, L. Xiao, and D. A. Weitz, arXiv (2021).
- [31] D. Fragedakis, E. Chaparian, and O. Tammisola, *Journal of Fluid Mechanics* **911**, A58 (2021).
- [32] L. T. Akanji and S. K. Matthai, *Transport in porous Media* **81**, 241 (2010).
- [33] S. S. Datta, H. Chiang, T. Ramakrishnan, and D. A. Weitz, *Physical Review Letters* **111**, 064501 (2013).
- [34] C.-h. Liu, S. R. Nagel, D. Schecter, S. Coppersmith, S. Majumdar, O. Narayan, and T. Witten, *Science* **269**, 513 (1995).
- [35] S. Coppersmith, C.-h. Liu, S. Majumdar, O. Narayan, and T. Witten, *Physical Review E* **53**, 4673 (1996).
- [36] S. A. Ocko and L. Mahadevan, *Physical review letters* **114**, 134501 (2015).
- [37] N. J. Derr, D. C. Fronk, C. A. Weber, A. Mahadevan, C. H. Rycroft, and L. Mahadevan, *Physical Review Letters* **125**, 158002 (2020).
- [38] L. N. Reddi, X. Ming, M. C. Hajra, and I. M. Lee, *Journal of Geotechnical and Geoenvironmental Engineering* **126**, 236 (2000).

Temporal Evolution in the Networks of Porous Materials: From Homogenization to Instability

Ahmad Zareei, Pan Deng, and Ariel Amir*

School of Engineering and Applied Sciences, Harvard University, Cambridge, MA, 02148

(Dated: February 23, 2021)

0. 61. SIMULATION ALGORITHM

In our simulations, we tested two kinds of networks: (i) diamond-grid network, and (ii) topologically random network. In the diamond-grid network, we choose $N_x = 200$ edges in the horizontal direction and $N_y = 100$ edges in the vertical direction. The random network is created using $N_x \times N_y$ uniformly distributed points where the connection between the nodes are obtained using Delaunay triangulation. The diameter of each edge is sampled from either a uniform distribution in $r \in [1, 14]$, log-normal distribution with $\mu = 3, \sigma = 0.48$, or truncated normal distribution with $\mathcal{N}(\mu = 7.0, \sigma = 3.6)$. The external flow pressure is applied horizontally from left to right. An external pressure is then assumed between the left most nodes and the right most nodes ($p_{\text{left}} = 10, p_{\text{right}} = 0$). Assuming a Poiseuille flow in each edge, the fluid flow q and pressure difference δp_e in each edge is related through $q_e = C_e \delta p_e$, where $C_e = \pi r_e^4 / 8\mu L_e$, and L_e is the length of the tube, μ is the viscosity of the fluid. Let Δ be the network's oriented incidence matrix. Define $|q_e\rangle$ as the vector of flow through all the edges, then we have

$$|q_e\rangle = C_e \Delta |p_i\rangle, \quad \text{and} \quad (S1)$$

where $|p_i\rangle$ is the vector of pressure of all nodes. With a given boundary condition, we solve the equation through modified nodal analysis method. The conservation of mass at each node can be written as

$$|q_n\rangle = \Delta^\top \mathbf{C} \Delta |P_n\rangle \quad (S2)$$

where $\mathbf{C} = \text{diag}(C_e^{(1)}, C_e^{(2)}, \dots, C_e^{(N_e)})$ is a diagonal matrix of edge conductances, and Δ is the network oriented incidence matrix, $|p_n\rangle$ is the vector of pressure at the nodes, and $|q\rangle_n$ is the vector of total incoming flow to the nodes. Note that total incoming flow to an internal node is zero due to the conservation of mass, and is some non-zero value at the boundary nodes. As a result we can partition the governing equation (Eq. (S2)) to obtain

$$\begin{bmatrix} \Delta_b^\top \mathbf{C} \Delta_b & \Delta_b^\top \mathbf{C} \Delta_n \\ \Delta_n^\top \mathbf{C} \Delta_b & \Delta_n^\top \mathbf{C} \Delta_n \end{bmatrix} \begin{bmatrix} P_1^{BC} \\ P_2^{BC} \\ \vdots \\ P_n \\ \vdots \\ P_{N_n} \end{bmatrix} = \begin{bmatrix} q_1 \\ q_2 \\ \vdots \\ 0 \\ \vdots \\ 0 \end{bmatrix} \rightarrow \begin{bmatrix} \mathbf{A}_{bb} & \mathbf{A}_{bn} \\ \mathbf{A}_{nb} & \mathbf{A}_{nn} \end{bmatrix} \begin{bmatrix} P_1^{BC} \\ P_2^{BC} \\ \vdots \\ P_n \\ \vdots \\ P_{N_n} \end{bmatrix} = \begin{bmatrix} q_1 \\ q_2 \\ \vdots \\ 0 \\ \vdots \\ 0 \end{bmatrix} \quad (S3)$$

where $\mathbf{A}_{st} = \Delta_s^\top \mathbf{C} \Delta_t^\top$ and $s, t \in \{a, b\}$. In summary the above equations simplifies to

$$\begin{cases} \mathbf{A}_{bb} |P_{BC}\rangle + \mathbf{A}_{bn} |P_n\rangle = |q\rangle \\ \mathbf{A}_{nb} |P_{BC}\rangle + \mathbf{A}_{nn} |P_n\rangle = 0 \end{cases} \quad (S4)$$

$$\mathbf{A}_{nn} |P_n\rangle = -\mathbf{A}_{nb} |P_{BC}\rangle \quad (S5)$$

Solving the above equation results in the pressure field on the nodes and the fluid flux at the boundary nodes. With the solution of q_e , the increase (decrease) of tube radius under erosion (clogging) law is

$$\frac{dr_e}{dt} \propto \frac{q_e}{r_e^n}. \quad (S6)$$

We use simple forward Euler to integrate the equations. For each iteration, we choose the time step dt so that $\max(dr) = 0.1r_0$, where r_0 is the average initial radius of all edges.

* arielamir@seas.harvard.edu

*Let's discuss... I usually solve this differently,
though the two approaches
must be equivalent.*

S2. ADDITIONAL NUMERICAL RESULT

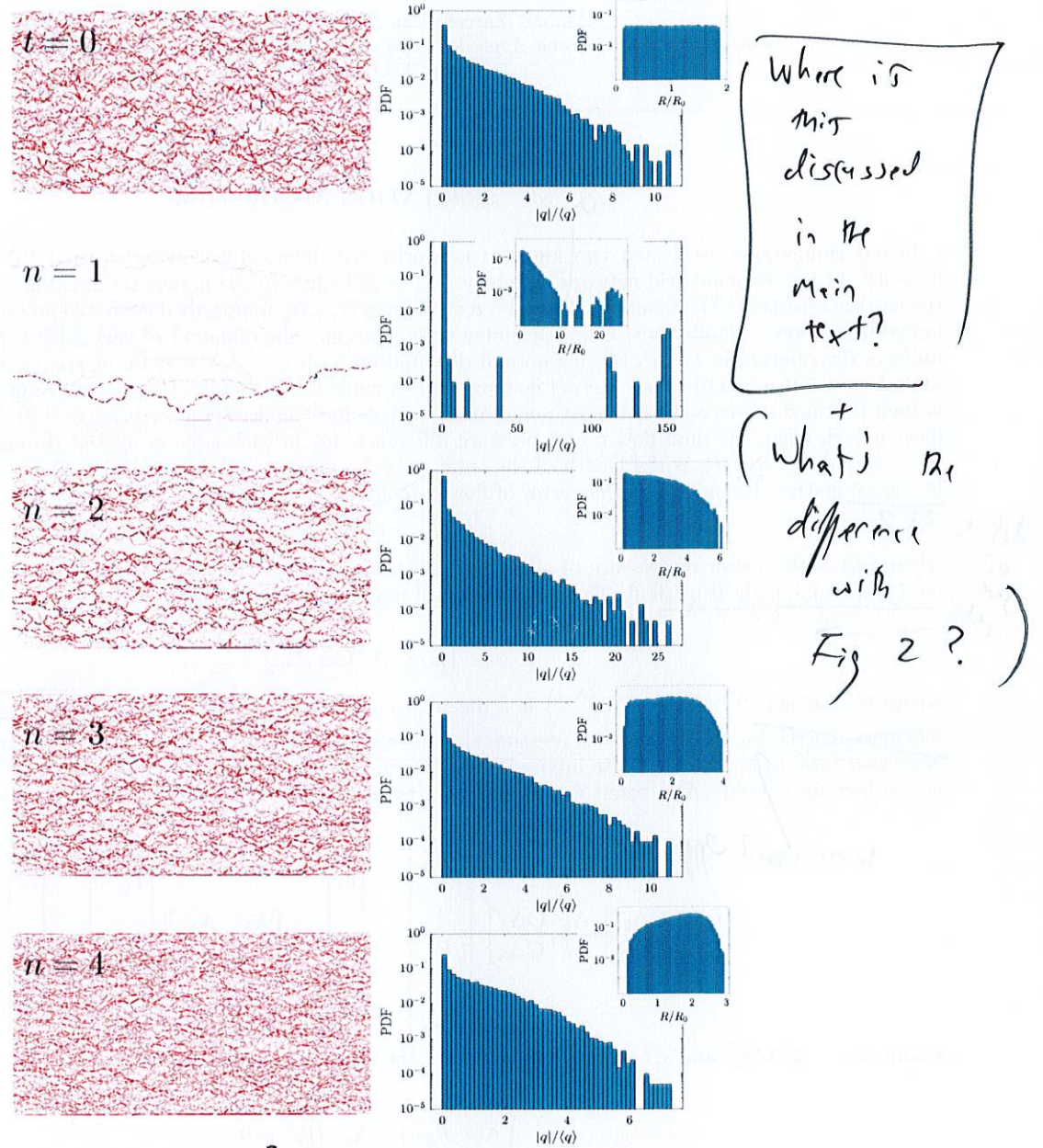


FIG. S1. Erosion in a network of randomly posed pipes. The initial condition is shown with the label $t = 0$ in the first row. Each row afterward corresponds to the simulation result after N steps such that $\langle R_{t=N} \rangle = 2R_0$ where $R_0 = \langle R_{t=0} \rangle$; in other words the same amount of material is eroded in all cases. The erosion laws used here is $dR/dt = \alpha Q/R^n$ where n varies for each row. The constant α in all cases are 1 and time step dt is chosen such that the maximum amount of increase in R at each step is smaller than $0.01R_0$.

not finite?

? in main text?

Why do we need this section? \Rightarrow Are there new results here?

S3

S3. ANALYTICAL RESULTS

In order to describe the universality of fluid flow distribution, we introduce the following model based on [1]. We consider a structured diamond grid as shown in Fig. S2, and denote the total flow to node i at level L inside by $Q(L, i)$. This incident flow to no the node is then redistributed to the neighboring nodes at level $L + 1$. We assume

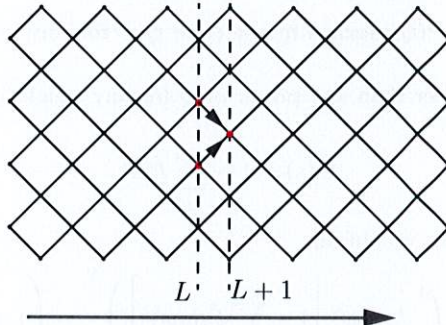


FIG. S2. Schematic of diamond grid.

that this redistribution is done by weights w_{ij} where

$$Q(L + 1, j) = \sum_i w_{ij} Q(L, i) = w_{i,i+1} Q(L, i+1) + w_{i,i} Q(L, i). \quad (\text{S7})$$

Note that since the total mass is conserved, then $\sum_j w_{ij} = 1$. Next, we assume that the weights w_{ij} are drawn from a distribution $\eta(w)$. Since $\eta(w)$ is a distribution, then $\int \eta(w) dw = 1$. Furthermore, since $\sum_j w_{ij} = 1$, we can conclude that

$$\sum_j w_{ij} = 1 \rightarrow N E[w_{ij}] = 1 \rightarrow E[w_{ij}] = 1/N \rightarrow \int w \eta(w) dw = 1/N \quad (\text{S8})$$

Assuming a general distribution of $\eta(w)$, we can use the mean-field approximation to find the distribution of Q at the layers. The values of $Q(L, i)$ are not independent for neighboring sites; however, in our mean field approximation we ignore such correlations. We have

$$P_L(Q) = \prod_{j=1}^N \left\{ \int_0^1 dw_j \eta(w_j) \int_0^\infty dQ_j P_{L-1}(Q_j) \right\} \times \delta \left(\sum_j w_j Q_j - Q \right) \quad (\text{S9})$$

The constraint that Q 's emanating downward should add up to one is in the definition of $\eta(w)$. The only approximation in the above equation is that we neglect the possible correlation between the values of Q among ancestors. If we take the Laplace transform of the above equation, we obtain

$$\tilde{P}(s) \equiv \int_0^\infty P(Q) e^{-Qs} dQ \quad (\text{S10})$$

$$\tilde{P}(s) = \int_0^\infty \prod_{j=1}^N \left\{ \int_0^1 dw_j \eta(w_j) \int_0^\infty dQ_j P(Q_j) \right\} \times \delta \left(\sum_j w_j Q_j - Q \right) e^{-Qs} dQ \quad (\text{S11})$$

$$= \left(\int_0^1 dw \eta(w) \tilde{P}(sw) \right)^N \quad (\text{S12})$$

Or in summary

$$\boxed{\tilde{P}(s) = \left(\int_0^1 dw \eta(w) \tilde{P}(sw) \right)^N} \quad (\text{S13})$$

Note that in the above equation N determines the number of neighboring sites and in our structured diamond grid $N = 2$. The above equation recursively converges to a distribution. If we set $\eta(w) = \delta(w - 1/2)$, then the flow at each node has probability of $1/2$ to move to either of the neighboring sites. As a result the flow at a given depth L will become homogeneous as $P_L(Q) = \delta(Q - \bar{Q})$ where \bar{Q} is the average of input fluid flow. This results is the same as having the same diameter for all the edges which results in a singular solution in the structured grid.

$P(Q)$ decays faster than Q^{-n} for any n

We first show that $P(Q)$ decays faster than any power of Q for any weight distributions. We expand the Laplace transform using a Taylor expansion as

$$\tilde{P}(s) = 1 + \sum_j \tilde{P}_j s^j. \quad (\text{S14})$$

Inserting this expansion into Eq. (S13), we obtain

$$1 + \sum_j \tilde{P}_j s^j = \left(\int_0^1 dw \eta(w) \left[1 + \sum_j \tilde{P}_j (sw)^j \right] \right)^N = \left(1 + \sum_j \tilde{P}_j \langle w^j \rangle s^j \right)^N \quad (\text{S15})$$

where $\langle w^j \rangle = \int_0^1 \eta(w) w^j dw$ is the j -th moment of the weights w . In the above equation we can observe that

$$P_j (N \langle w^j \rangle - 1) = G(P_{j-1}, P_{j-1}, \dots, P_1) \quad (\text{S16})$$

In the above equation P_j can only diverge only if $N \langle w^j \rangle - 1 = 0$. If w can only be zero and one, then $\langle w^j \rangle = \langle w \rangle = 1/N$ and the coefficient can become zero! Other than this special distribution, when $0 < w < 1$, then

$$w \in [0, 1] \rightarrow w > w^2 > w^3 > \dots \quad (\text{S17})$$

$$\forall k > 1 \rightarrow \langle w^k \rangle < \langle w \rangle = \frac{1}{N} \quad (\text{S18})$$

which means that $N \langle w^j \rangle - 1 \neq 0$ and as a result P_j is finite. P_j on the other hand is the j -th moment or $\langle Q^j \rangle$ and it is finite. If $P \approx Q^{-n}$, then the n -th moment will not be finite i.e. $\langle Q^{n+1} \rangle = P_{n+1}$ is not finite. We can then conclude that $P(Q)$ should go to zero faster than any Q^{-n} as $Q \rightarrow \infty$! In other words $d \log P(Q)/d \log Q \rightarrow -\infty$ as $Q \rightarrow \infty$.

Exponential Decay

The main recursive governing equation for a diamond grid is

$$\tilde{P}(s) = \left(\int_0^1 dw \eta(w) \tilde{P}(sw) \right)^2 \quad (\text{S19})$$

At each node there are two neighboring nodes where the flux is distributed by w_1 and w_2 among them. Assuming that w_1 is uniformly distributed between 0 and 1, then $w_2 = 1 - w_1$ (due to conservation of mass $w_1 + w_2 = 1$). Now $\eta(w)$ can be obtained using

$$\eta(w) = M \int_0^1 dw_1 \delta(1 - w_1 - w) = M, \quad (\text{S20})$$

$$\text{since } \int_0^1 \eta(w) dw = 1 \rightarrow M = 1 \quad (\text{S21})$$

$$\eta(w) = 1 \quad (\text{S22})$$

Just for completeness, if there are three neighboring connections ($N = 3$), then we have

$$\eta(w) = M \int_0^1 dw_1 \int_0^1 dw_2 \delta(1 - w_1 - w_2 - w) \quad (\text{S23})$$

$$= M(1 - w) \rightarrow \int_0^1 \eta(w) dw = 1 \rightarrow M = \frac{1}{2} \quad (\text{S24})$$

$$\eta(w) = \frac{1}{2}(1 - w) \quad (\text{S25})$$

As a result Eq. (S19) simplifies to

$$\tilde{P}(s) = \left(\int_0^1 dw \tilde{P}(sw) \right)^2 \quad (S26)$$

In order to solve the above equation, we assume $\tilde{V}(s) = \sqrt{\tilde{P}(s)}$.

$$\tilde{V}(s) = \int_0^1 dw \tilde{V}(sw) = \int_0^s \frac{du}{s} \tilde{V}^2(u) \quad (S27)$$

$$s\tilde{V}(s) = \int_0^s du \tilde{V}^2(u) \quad (S28)$$

$$(S29)$$

Taking the differentiation with respect to s yields

$$\tilde{V}(s) + s \frac{d\tilde{V}(s)}{ds} = \tilde{V}^2(s) \quad (S30)$$

$$\frac{d\tilde{V}}{\tilde{V}^2 - \tilde{V}} = \frac{ds}{s} \quad (S31)$$

$$\log\left(\frac{1 - \tilde{V}}{\tilde{V}}\right) = \log(s) \quad (S32)$$

$$\tilde{V}(s) = \frac{1}{1 + Cs} \quad (S33)$$

We set the mean to 1 i.e.,

$$\int_0^\infty Q P(Q) dQ = 1 \rightarrow \frac{d\tilde{P}}{ds}|_{s=0} = -1 \quad (S34)$$

$$\frac{d\tilde{V}}{ds} = \frac{1}{2\sqrt{\tilde{P}(s)}} \frac{d\tilde{P}(s)}{ds} \rightarrow \frac{d\tilde{V}(s)}{ds}|_{s=0} = \frac{-1}{2} \quad (S35)$$

$$\frac{d\tilde{V}(s)}{ds} = \frac{-C}{(1 + Cs)^2}|_{s=0} = -C = \frac{-1}{2} \rightarrow C = \frac{1}{2} \quad (S36)$$

As a result, we have

$$\tilde{P}(s) = \left(\frac{1}{1 + s/2} \right)^2 \quad (S37)$$

$$P(Q) = 4Qe^{-2Q} \quad (S38)$$

We can then show that for a uniform distribution of w 's, the PDF of Q 's become an exponential tail. For other distribution of w 's, we similarly find a similar trend which can be seen in the numerical simulations. w . Note that in the distribution with exponential tail, the only parameter that determines the the PDF of the average fluid flow. This shows that why we observe the universal behaviour for the PDF of normalized fluid flux where the average of normalized fluid flux is unity.

S4. CLOGGING BEHAVIOR AT INITIAL TIMES

Considering a small change in the radius of edges, and as a result the conductance of the edges $\mathbf{C} + \delta\mathbf{C}$, usign Eq. (S5) we find that

$$|P'\rangle = |P\rangle - (\Delta_n^\top \mathbf{C} \Delta_n)^{-1} [(\Delta_n^\top \delta\mathbf{C} \Delta_n) |P\rangle + (\Delta_n^\top \delta\mathbf{C} \Delta_b) |P_{BC}\rangle] \quad (S39)$$

where we used the fact that

$$(\mathbf{A} + \delta\mathbf{A})^{-1} = \mathbf{A}^{-1} - (\mathbf{A}^{-1} \delta\mathbf{A}) \mathbf{A}^{-1} + (\mathbf{A}^{-1} \delta\mathbf{A})^2 \mathbf{A}^{-1} + \dots \quad (S40)$$

Calculating for the changes in the fluid flux, we find that

$$|q'\rangle = (\mathbf{C} + \delta\mathbf{C}) (\Delta_b |P_{BC}\rangle + \Delta_n |P'\rangle) \quad (S41)$$

$$= |q\rangle + \delta\mathbf{C} \mathbf{C}^{-1} |q\rangle - \mathbf{C} \Delta_n (\Delta_n^\top \mathbf{C} \Delta_n)^{-1} [(\Delta_n^\top \delta\mathbf{C} \Delta_n) |P\rangle + (\Delta_n^\top \delta\mathbf{C} \Delta_b) |P_{BC}\rangle] \quad (S42)$$

The above equation can then be used to study the evolution of order parameter in the networks. Note that during the blockage of pore-throats the matrix Δ changes.

- [1] C.-h. Liu, S. R. Nagel, D. Schecter, S. Coppersmith, S. Majumdar, O. Narayan, and T. Witten, Force fluctuations in bead packs, *Science* **269**, 513 (1995).